Thermal Design and Analysis of Cooling SOFIA HIRMES to 4K Cryogenic Temperature using Cryocooler

Michael K. Choi[1]
NASA Goddard Space Flight Center, Greenbelt, MD 20771

HIgh Resolution Mid-infrarEd Spectrometer (HIRMES) is a facility-class instrument aboard the Stratospheric Observatory for Infrared Astronomy (SOFIA) Aircraft Observatory. A TransMIT PTD 406C pulse tube cryocooler is used to cool the optical bench and optical components to 4K. A second PTC is dedicated to cool the 3He/4He sorption cooler. The first stages of the PTCs share the heat load from the intermediate temperature stage. The second stage of the first PTC removes nearly all the heat load from the 4K stage. The results of thermal analysis show that the 4K stage of the HIRMES thermal subsystem meets all of its requirements using the 100% heat load margin approach and conservative modeling assumptions.

Nomenclature

ADR	=	Adiabatic Demagnetization Refrigerator
CRES	=	Corrosion RESistant steel
FPA	=	focal plane assembly
He	=	helium
HIRMES	=	HIgh Resolution Mid-infrarEd Spectrometer
PAM	=	pole amplitude modulation
PTC	=	pulse tube cryocooler
RRR	=	Residual Resistive Ratio
SOFIA	=	Stratospheric Observatory for Infrared Astronomy
MLI	=	multilayer insulation

I. Introduction

HIRMES is a facility-class instrument aboard the SOFIA aircraft observatory. Its primary science is to investigate protoplanetary disk physics with a focus on the evolution of distribution of oxygen, water ice, water vapor, and molecular hydrogen during planet formation. It is under development at NASA Goddard Space Flight Center (GSFC). Figure 1 shows the SOFIA aircraft observatory. HIRMES performs high sensitivity spectroscopy with resolving power from spectrophotometry up to approximately 100,000, covering the spectral range from 25-122 μm.[1] It will fly approximately two campaigns per year. Each campaign will last for 3-4 weeks, with multiple sorties during each. There will be approximately 24 total flights per year to add up to approximately 200-240 hours of actual science collection per year. The instrument delivery date is November 2019.

Figure 1. SOFIA aircraft observatory.

[1] Senior Aerospace Engineer, Heat Transfer, Mechanical System Division

HIRMES has a 4K maximum temperature limit requirement for the optical bench and optical components, and a 70 mK maximum temperature limit requirement for the focal plane array (FPA). It has very tight volume and mass constraints. Thermal design is challenging. Figure 2 and Figure 3 show the exterior and interior, respectively, of HIRMES.[1] Pulse tube cryocooler #1 (PTC1) is used to cool the optical bench and optical components. An Adiabatic Demagnetization Refrigerator (ADR) is used to cool the FPA. A 3He/4He sorption cooler at ~300 mK is used to intercept heat for the Kevlar suspension assemblies that support the ADR salt pill and FPA. The 4He portion of the sorption cooler is used to pre-cool the ADR salt pill to 0.8 K before demagnetization. A 4He cooler is used to cool the 1 K baffle. During power cycling of the 3He/4He cooler, its condenser temperature requirement is 4K or colder. The power dissipation of the 3He/4He cooler is too high for PTC1 alone to meet this requirement. Therefore, PTC #2 (PTC2) has been added after the Critical Design Review. The second stage of PTC2 is dedicated to cool the condenser of the 3He/4He sorption cooler. The first stage of PTC2 is used to supplement the first stage of PTC1. This paper is in conjunction with thermal design and analysis of the 4K stage of the HIRMES thermal subsystem.

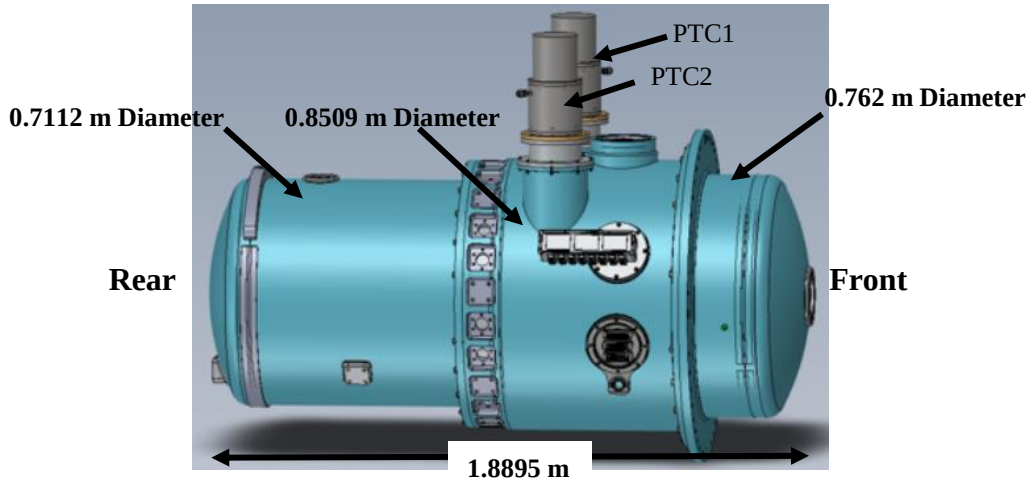

Figure 2. Exterior of HIRMES. (Credit: SOFIA HIRMES project)

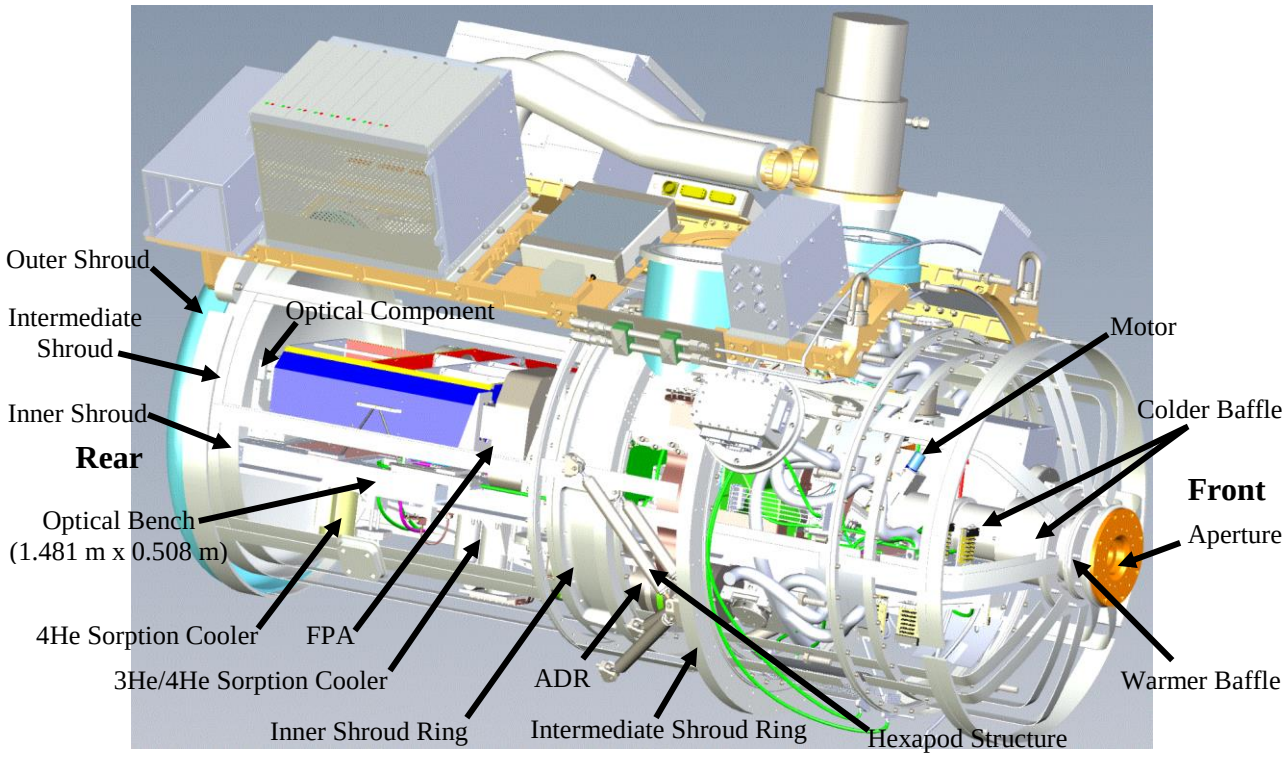

Figure 3. Interior of HIRMES. (Credit: SOFIA HIRMES project)

PTC1

Referring to Figures 2 and 3, HIRMES has three shrouds that enclose the optical bench and optical components. They are made of aluminum alloy 6061-T6 and are irridited. The exterior of the outer shroud is exposed to the SOFIA aircraft cabin air, which is at approximately 297K. The HIRMES avionics and cryocooler motor mounts are mounted to the outer shroud. There is an electrical harness from the avionics to the 4K regime. The second stage of PTC1 provides cooling to the inner shroud. The cold tip of the second stage is thermally coupled to an inner shroud ring by a copper strap. The inner shroud ring is mounted to the inner shroud. The first stage of PTC1 provides cooling to the intermediate shroud. The cold tip of the first stage is thermally coupled to an intermediate shroud ring by a copper strap. The intermediate shroud ring is mounted to the intermediate shroud. Both the intermediate shroud ring and inner shroud ring are made of aluminum alloy 6061-T6 and are irridited. The optical bench and optical components are also made of aluminum alloy 6061-T6 and are irridited. The optical bench is mounted to the inner shroud ring. A hexapod structure, which consists of titanium alloy Ti-6Al-4V struts, provides mechanical support for the shrouds and optical bench. It also provides thermal isolation between the inner and intermediate shrouds, and between the intermediate and outer shrouds. The location of the hexapod structure is shown in Figure 3. Figure 4 shows the hexapod structure between the inner and intermediate shrouds.

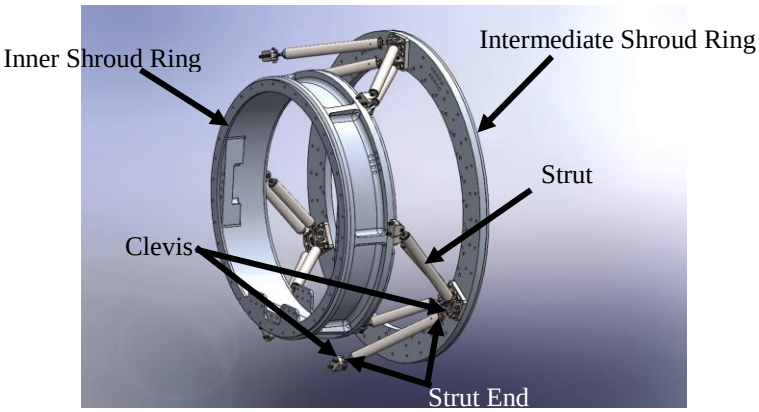

Figure 4. Hexapod structure between inner and intermediate shrouds. (Credit: SOFIA HIRMES project)

The hexapod structure transfers heat by solid conduction through the Ti-6Al-4V struts, CRES 416 strut ends, and CRES 303 clevises, and by conduction through the contacts at the clevises and strut ends.

HIRMES has a 7.62 cm (3 inch) diameter aperture at the front end. It views an approximately 240K (-33°C) ambient air outside the SOPHIA aircraft. The baffle of the aperture (Figure 3) is designed to minimize the heat load to the 4K regime. The wamer baffle interior has a good view to the outside ambient through the aperture. It is mounted to the intermediate shroud and sinks heat to it. The colder baffle encloses the warmer baffle and extends to the optical bench. It is mounted to the inner shroud and sinks heat to it. The view factor from the colder baffle interior to the outside ambient through the aperture is very small. The Vantablack® super-black coating on the interior of the baffles minimizes stray light.

Table 1 presents the current best estimates for the HIRMES mass for each of the three temperature regimes. They affect the transient temperature response, such as during power outage, motor turn on, and initial cooldown from 297K to steady state temperatures. Specific heat also affects the transient temperature response. The specific heats of the HIRMES materials decrease when the temperature decreases. Figure 5 shows the specific heat versus temperature for selected materials.[2] The specific heat of aluminum alloy 6061-T6 at 4K is only 0.3 $Jkg^{-1}K^{-1}$, which is 0.03% of that at 300K. Table 2 is a summary of the electrical harness that has thermal implications. The total number of conductors is 1,114.

Table 1. Mass Estimates for HIRMES.

	Mass (kg)	Mass by Material (kg)
Inner Shroud Components	208.9	Al: 175.8; Cu: 19.5 (straps); manganin: 7.8 (harness); Ti-6Al-4V: 0.54 (hexapods); CRES: 5.31 (hexapods and harness);
Intermediate Shroud Components	49.8	Al: 44.7; manganin: 1.3 (harness); Ti-6Al-4V: 0.8 (hexapods); CRES: 1.4 (hexapods and harness)
Outer Shroud Components	436.6	Al 6061-T6: 419.1; Cu: 17.5

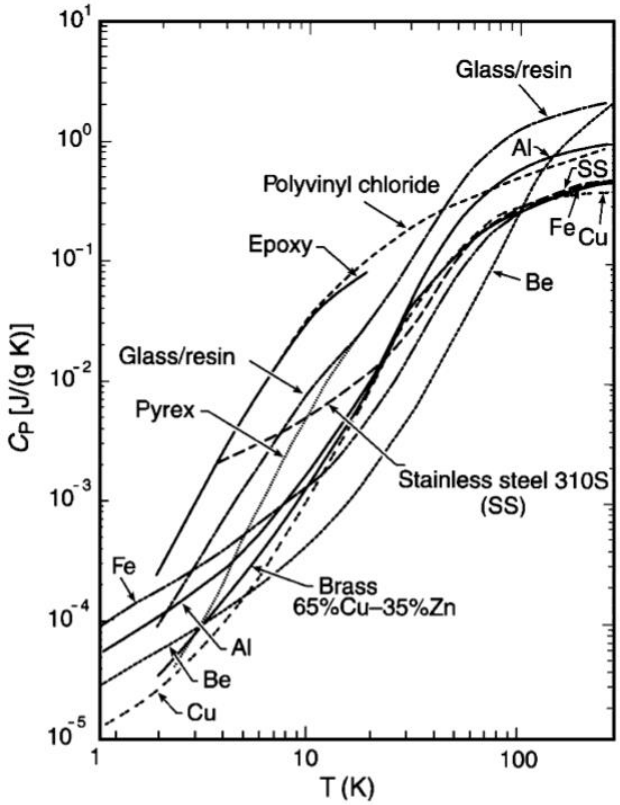

Figure 5. Effect of temperature on specific heat. (Reprinted from Ekin[2])

Table 2. HIRMES Electrical Harness.

Type	Number of Conductors	Length (cm)			
		Total	Between Outer and Intermediate Shrouds	Between Intermediate and Inner Shrouds	Within Inner Shroud
32 AWG, Stainless Steel Coax	24	124.46	20.32	15.24	88.9
32 AWG, Stainless Steel Coax	24	116.84	20.32	15.24	81.28
36 AWG, Manganin Shield Twisted Pair	12	113.03	20.32	15.24	78.74
26 AWG, Stainless Steel Twisted Pair	20	121.92	20.32	15.24	86.36
36 AWG, Manganin Shield Twisted Pair	4	132.08	20.32	15.24	96.52
32 AWG, Stainless Steel Coax	6	124.46	20.32	15.24	88.9
36 AWG, Manganin Unshielded	700	279.4	20.32	15.24	243.84
44 SWG, Manganin Twisted Pair	300	154.94	20.32	15.24	119.38
32 SWG, Manganin Twisted Pair	24	154.94	101.6	25.4	27.94

II. Cryocooler Load Map and Thermal Design Goal

Figure 6 presents the TransMIT PTD 406C cryocooler load map provided by the manufacturer. It drives the methodology of thermal analysis in conjunction with margin. Without any heat load to the first and second stages, the temperatures of the cold tips for the first stage and second stage are 36.5K and 2.15K, respectively. The goal of thermal design and analysis is to achieve a maximum steady state temperature prediction of 3.6K for the optical bench and optical components. It assures the temperatures of the optical bench and optical components remain below the 4K thermal requirement when a motor is turned on for up to 90 seconds and dissipates up to 400 mW.

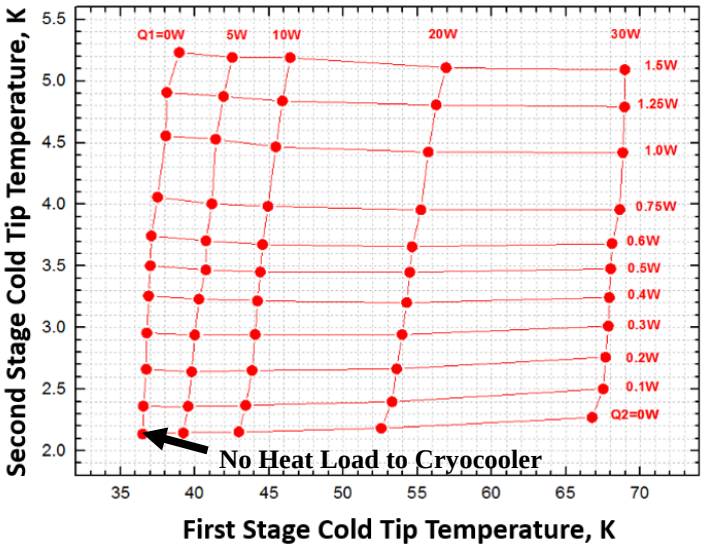

Figure 6. HIRMES PTC load map.

III. Thermal Design

Thermal conductivity affects conductance, which in turn affects conduction heat transfer. As the temperature decreases, the thermal conductivities of some of the materials, such as aluminum alloy 6061-T6, used in the HIRMES mechanical design decrease. Figure 7 shows this effect on selected materials.[3] For a given amount of heat transfer by conduction, a lower thermal conductivity leads to a larger temperature gradient.

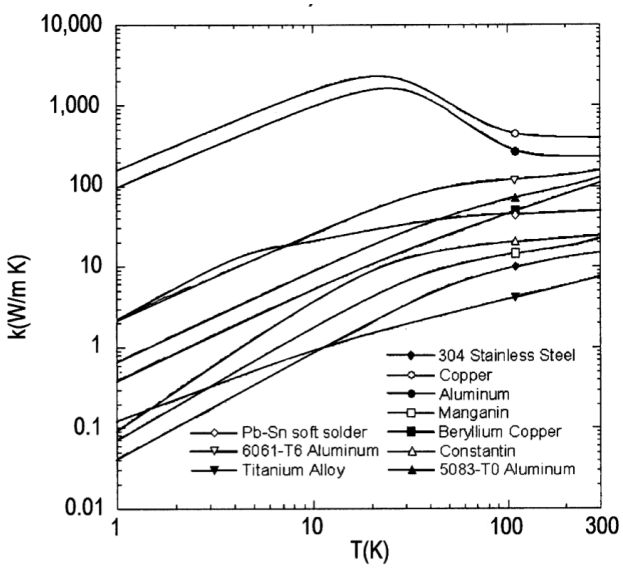

Figure 7. Effect of temperature on thermal conductivity of metals. (Reprinted from CRYOCOMP®[3])

At 4K, the thermal conductivity of aluminum alloy 6061-T6 is only 10 $Wm^{-1}K^{-1}$,[4] which is close to that of titanium alloy Ti-6Al-4V at 300K.

Figure 8 shows the thermal conductivity versus temperature at different purities of copper,[5] which is considered for thermal straps on HIRMES.

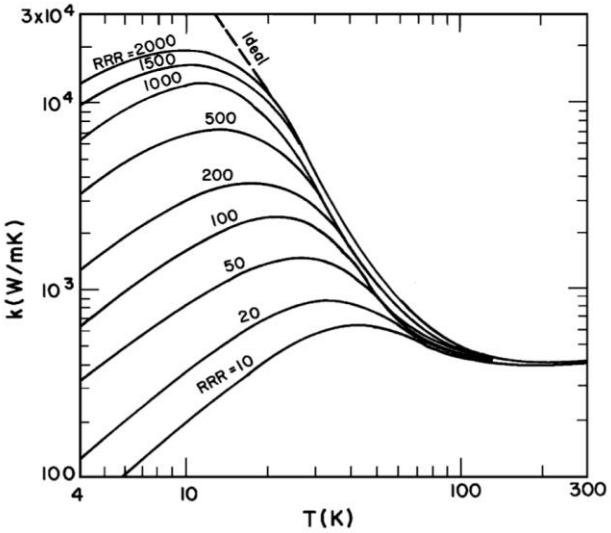

Figure 8. Thermal conductivity versus temperature of different purities of copper (Reprinted from Powell and Fickett[5]).

There are a large number of thermal contacts on HIRMES. Figure 9 shows thermal contact conductance versus temperature for 1 cm^2 area and a variety of contact preparations and conditions.[2] Contact pressure also affects thermal contact conductance. For example, from Figure 10, at 4K, the thermal contact conductance of the Au-Au joint with a 50 kg force is nearly 5 times that with a 10 kg force.

To maximize the thermal contact conductances at the critical joints on HIRMES, both sides of these joints are gold plated. This method of maximizing thermal contact conductance at cryogenics temperatures of about 4K has flight heritage at GSFC. With a bolt force of 3,000-10,000 N, a contact conductance of 0.6-0.69 WK^{-1} per bolt was measured by GSFC in the Hitomi (formerly ASTRO-H) project, and is deemed conservative. If neither side of the joint is gold plated, the contact conductance is an order of magnitude smaller (i.e., 0.06-0.069 WK^{-1} per bolt).

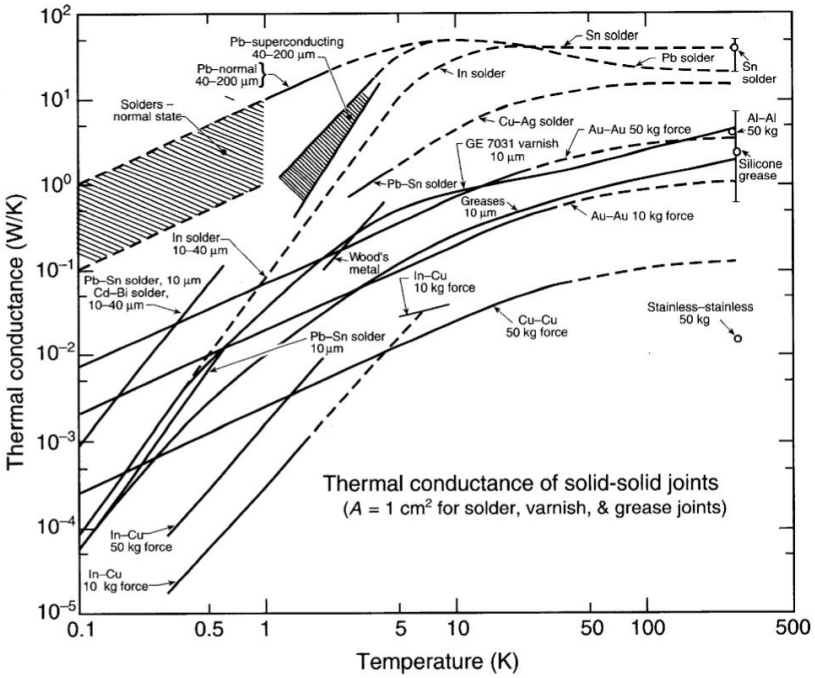

Figure 9. Thermal contact conductance versus temperature for 1 cm^2 area and a variety of contact preparations and conditions. (Reprinted from Ekin[2])

The HIRMES thermal design approach to meet the 4K maximum temperature limit requirement for the optical bench and optical components is to:

•Maximize the thermal conductance between the PTC1 second stage cold tip and the inner shroud ring.

•Maximize the thermal conductance between the PTC2 second stage cold tip and the 3He/4He sorption cooler.

•Maximize the thermal conductance between the inner shroud ring and the optical bench and optical components.

•Maximize the circumferential thermal conductance for the inner shroud ring.

•Maximize the longitudinal thermal conductance for the inner shroud.

•Minimize the conductive and radiative parasitic heat loads for the 4K regime.

•Maximize the thermal conductance between PTC first stage cold tips and intermediate shroud ring.

•Maximize the circumferential thermal conductance for the intermediate shroud ring.

•Maximize the longitudinal thermal conductance for the intermediate shroud.

•Minimize the radiative parasitic heat loads for the intermediate shroud and intermediate shroud ring.

A thermal model is used for thermal iterations in the thermal design process to meet the 4K thermal requirement. It has incorporated the above thermal design approach. Details of the thermal model are presented in Section IV.

A. Method of Maximizing Thermal Conductance between PTC Cold Tips and Shroud Rings

Figure 10 shows the thermal straps for the cold tips of the PTC1 first and second stages.

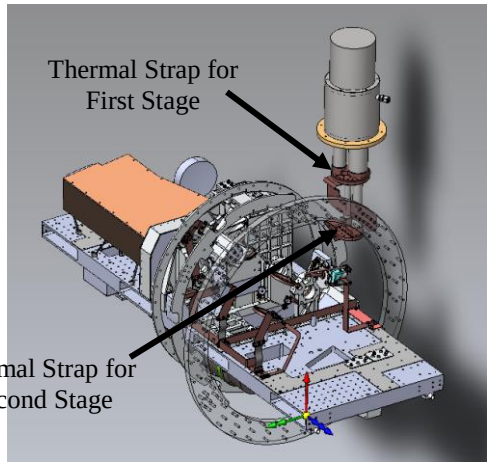

Figure 10. PTC1 thermal straps. (Credit: SOFIA HIRMES project)

To maximize the thermal conductance between the PTC1 second stage cold tip and the inner shroud ring, a high purity (RRR=1,000) copper strap is used after thermal iterations. Its ratio of area to length (A/L) is 0.001676 m. At 4K, its conductivity is approximately 6,240 $Wm^{-1}K^{-1}$.[6] It is twice as much as that of a lower purity (RRR=500) copper strap.[6] Another factor used in the RRR selection is that it can be degraded by impurities and processing steps. A RRR of 1,000 is selected to meet the 4K thermal requirement for the optical bench and optical components, despite it is more expensive. Copper is selected for flexible thermal straps because of its flight heritage, including Hitomi (formerly ASTRO-H), at GSFC. Conservative thermal contact conductances of 3.3 WK^{-1} and 2 WK^{-1} are assumed for the joints at the cold tip and inner shroud ring, respectively, after thermal iterations. To achieve them, the surfaces of the copper strap, inner shroud ring, and cold tip at the joints are gold plated. An adequate number of bolts, with a bolt force of 3,000-10,000 N each, are used at each joint to assure a good contact pressure. Based on the size and number of bolts, the contact pressure is estimated. The same method is used for the thermal conductance between the PTC2 second stage cold tip and the 3He/He4 sorption cooler condenser busbar.

To maximize the thermal conductance between the PTC1 first stage cold tip and the intermediate shroud ring, a high purity (RRR=500) copper strap is used after thermal iterations. Its ratio of A/L is 0.001676 m. At 50K, which is approximately the temperature goal, its thermal conductivity is approximately 1,020 $Wm^{-1}K^{-1}$.[6] If a higher purity (RRR=1,000) copper strap is used, it merely increases the thermal conductivity to 1,210 $Wm^{-1}K^{-1}$ and is more expensive. Therefore, RRR 500 is selected. Conservative thermal contact conductances of 3 WK^{-1} and 2 WK^{-1} are assumed for the joints at the cold tip and intermediate shroud ring, respectively, after thermal iterations. To achieve them, the surfaces of the copper strap, intermediate shroud ring, and cold tip at the joints are gold plated. An adequate number of bolts, with a bolt force of 3,000-10,000 N each, are used at each joint to assure a good contact

pressure. Based on the size and number of bolts, the contact pressure is estimated. The same method is used for the thermal conductance between the PTC2 first stage cold tip and the intermediate shroud ring.

B. Method of Maximizing Circumferential Thermal Conductance for Shroud Rings

Because the inner shroud ring is made of aluminum alloy 6061-T6, its thermal conductance at 4K is very poor. Two high purity (RRR=1,000) aluminum doubler rings are used to increase its circumferential thermal conductance (Figure 11) after thermal iterations. Figure 12 presents the thermal conductivity of high purity (RRR=1,000) aluminum versus temperature used in the HIRMES thermal model.[4] At 4K, its thermal conductivity is approximately 3,000 $Wm^{-1}K^{-1}$. Doubler ring #1 has a 65.405 cm (25.75 inch) outer diameter and a 57.15 cm (22.5 inch) inner diameter. It is mounted to the front side of the inner shroud ring. Doubler ring #2 has a 62.865 cm (24.75 inch) outer diameter and a 57.15 cm (22.5 inch) inner diameter. It is mounted to the rear side of the inner shroud ring. Both doubler rings are 0.635 cm (0.25 inch) thick. A conservative thermal contact conductance of 5 WK^{-1} is assumed for each joint after thermal iterations. To achieve them, the surfaces of the doubler rings and inner shroud ring at the joints are gold plated. An adequate number of bolts, with a bolt force of 3,000-10,000 N each, are used at each joint to assure a good contact pressure. Figure 11 also shows these two doubler rings and the attachment location for the thermal strap of the PTC1 second stage cold tip. The thermal strap of the PTC2 second stage cold tip is attached to the 3He/4He sorption cooler busbar. The latter is thermally isolated from the optical bench by G10 standoffs. Therefore, the heat load removed by the PTC2 second stage from the 4K regime is negligibly small.

Two high purity (RRR=1,000) aluminum busbars thermally couple doubler ring # 1 to doubler ring #2 (Figure 11). Each busbar has a ratio of A/L of 3.5 x 10^{-4} m. A conservative contact conductance of 2 WK^{-1} is assumed for each joint after thermal iterations. To achieve them, the surfaces of the busbars and the doubler rings at the joints are gold plated. An adequate number of bolts, with a bolt force of 3,000-10,000 N each, are used at each joint to assure a good contact pressure. Based on the size and number of bolts, the contact pressure is estimated.

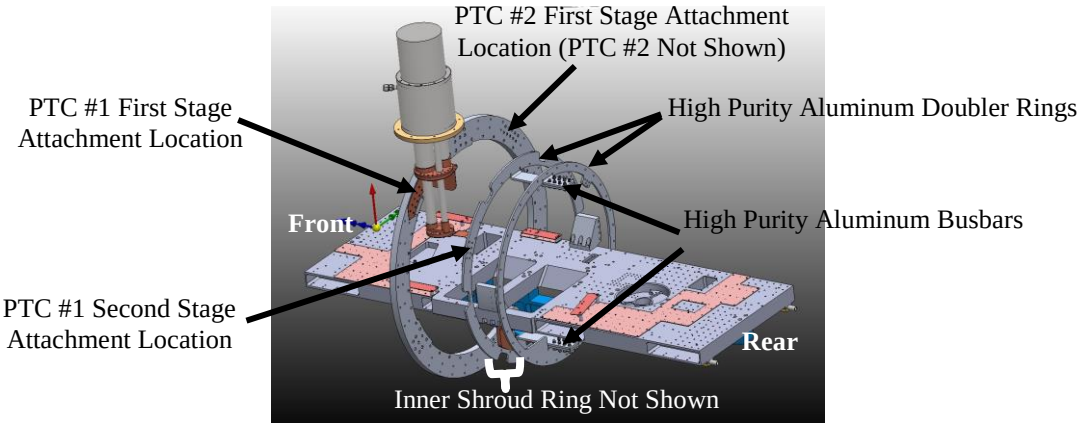

Figure 11. High purity aluminum doubler rings. (Credit: SOFIA HIRMES project)

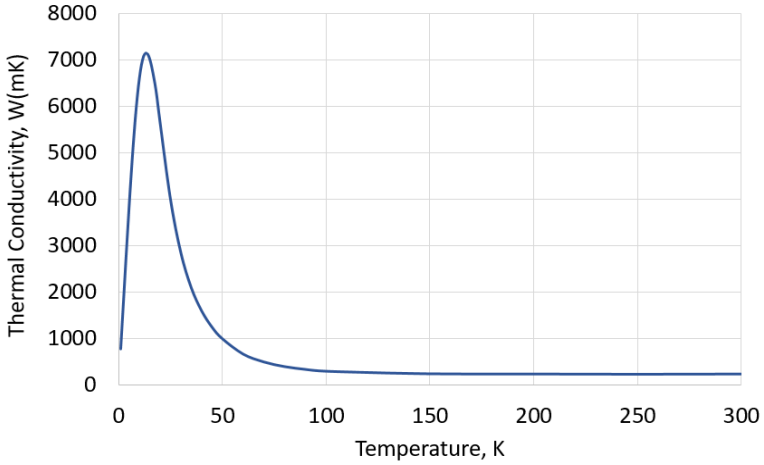

Figure 12. Effect of temperature on thermal conductivity of aluminum with RRR=1,000.[4]

Because the intermediate shroud ring is made of aluminum alloy 6061-T6, its thermal conductivity is only 50 $Wm^{-1}K^{-1}$ at 50K, which is the approximate temperature goal. A high purity (RRR=1,000) aluminum doubler ring is used to increase its circumferential thermal conductance after thermal iterations. It has a 81.026 cm (31.9 inch) outer diameter and a 70.866 cm (27.9 inch) inner diameter. It is mounted to the rear side of the intermediate shroud ring. The doubler ring is 0.635 cm (0.25 inch) thick. A conservative contact conductance of 5 WK^{-1} is assumed after thermal iterations. To achieve it, the surfaces of the doubler ring and intermediate shroud ring at the joint are gold plated. An adequate number of bolts, with a bolt force of 3,000-10,000 N each, are used at each joint to assure a good contact pressure. Based on the size and number of bolts, the contact pressure is estimated.Figure 11 also shows the attachment locations for thermal straps of the PTC1 and PTC2 first stage cold tips.

C. Method of Maximizing Thermal Conductance between Optical Components and Inner Shroud Ring

Because the optical bench and optical components are made of aluminum alloy 6061-T6, the conductances of these components at 4K are very poor. Two high purity (RRR=1,000) aluminum doublers on the optical bench are used to increase the lateral conductance at selected locations after thermal iterations. The first doubler is at the front, and the second one is at the rear. They are 0.635 cm (0.25 inch) thick, and are bolted to the optical bench. Figure 13 shows these two doublers. A conservative contact conductance of 2 WK^{-1} is assumed for each joint after thermal iterations. To achieve them, the contact surfaces of the doublers are gold plated. Gold foil is the thermal interface material between the doublers and the irritdited aluminum optical bench. An adequate number of bolts and adequate bolt forces are used at each joint to assure a good contact pressure. Additionally, a high purity (RRR=1,000) aluminum busbar thermally couples the front doubler to the rear doubler (Figure 14) after thermal iterations. It is 0.635 cm (0.25 inch) thick, and is located at the underside of the optical bench. A second high purity (RRR=1,000) aluminum busbar thermally couples the first high purity aluminum busbar to the inner shroud ring doubler (Figure 14). Its ratio of A/L is 7 x 10^{-4} m. A conservative contact conductance of 2 WK^{-1} is assumed for each joint after thermal iterations. To achieve them, the surfaces of the optical bench doublers, busbars, and inner shroud ring doubler at the joints are gold plated. An adequate number of bolts, with a bolt force of 3,000-10,000 N each, are used at each joint to assure a good contact pressure. Based on the size and number of bolts, the contact pressure is estimated.

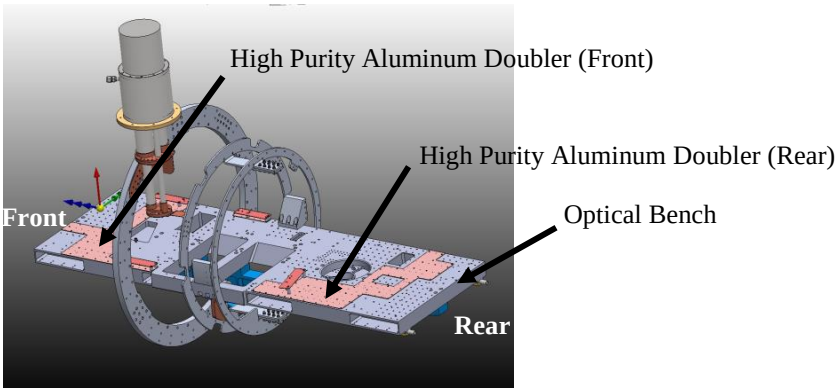

Figure 13. High purity aluminum doublers. (Credit: SOFIA HIRMES project)

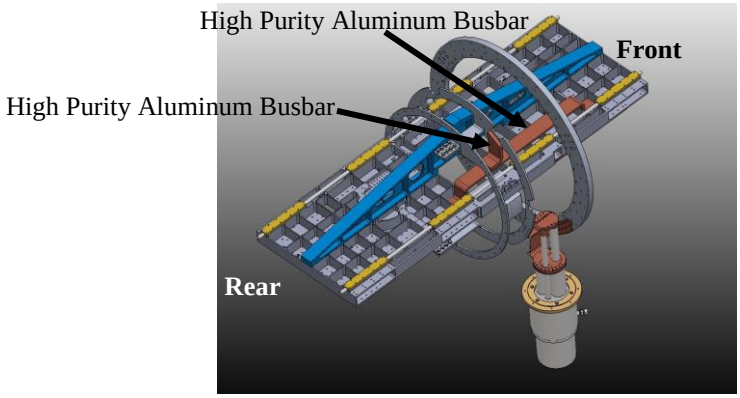

Figure 14. High purity aluminum busbars. (Credit: SOFIA HIRMES project)

There are seventeen optical components that have no power dissipation. At steady state, the ADR has micro watts of power dissipation. A copper (RRR=100) strap thermally couples each of the optical components and the ADR structure to either of the two high purity aluminum doublers on the optical bench after thermal iterations. The ratio of A/L of each copper strap is 3.8×10^{-5} m. Neither side of the joint is gold plated. Thermal interface material is not used. A conservative contact conductance of 0.2 WK^{-1} at the optical component or at the busbar is assumed after thermal iterations. To achieve them, an adequate number of bolts, with a bolt force of 3,000-10,000 N each, are used at each joint to assure a good contact pressure. Based on the size and number of bolts, the contact pressure is estimated.

D. Method of Maximizing Thermal Conductance between Motors and Inner Shroud Ring

There are nine motors. Each motor has up to 400 mW power dissipation when it is turned on. For three of the motors, a copper (RRR= 500) strap thermally couples each of them directly to the inner shroud ring doubler after thermal iterations. There are four high purity aluminum busbars for the remaining six motors. A copper (RRR= 500) strap thermally couples each of these six motors to the nearest high purity aluminum busbar (Figure 15) after thermal iterations. A copper (RRR=500) strap thermally couples each high purity aluminum busbar to the inner shroud ring doubler after thermal iterations. The ratio of A/L of each copper strap is 2.5×10^{-6} m. Conservative thermal contact conductances of 0.32 WK^{-1} at the shroud ring doubler or busbar, and 0.045 WK^{-1} at the motor are assumed after thermal iterations. Neither side of the joint is gold plated. Thermal interface material is not used. An adequate number of bolts, with a bolt force of 3,000-10,000 N each, are used at each joint to assure a good contact pressure. Based on the size and number of bolts, the contact pressure is estimated. The four high purity aluminum busbars for the motors are thermally isolated from the high purity aluminum doublers on the optical bench by G10 standoffs (Figure 15). This thermal isolation minimizes the heat conduction from the motors to the optical bench or optical components.

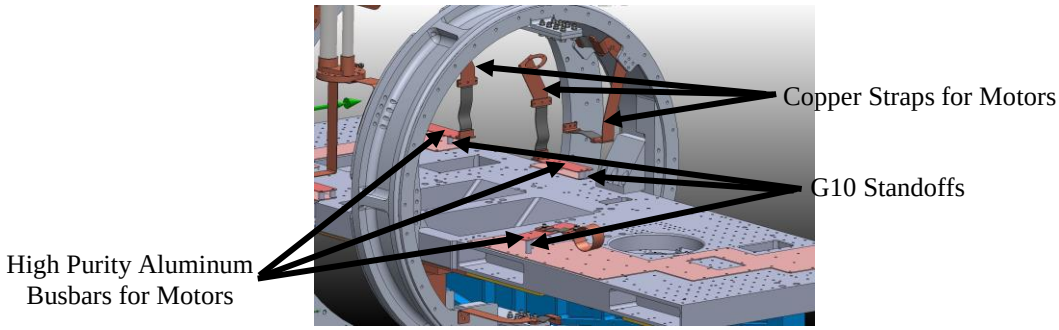

Figure 15. Copper straps and high purity aluminum busbars for motors. (Credit: SOFIA HIRMES project)

E. Method of Maximizing Longitudinal Thermal Conductance of Shrouds

Because the inner shroud is made of aluminum alloy 6061-T6, its conductance at 4K is very poor. As mentioned earlier, HIRMES has an aperture at the front end, and it views the ambient air of approximately 240K outside the SOFIA aircraft. There is a heat load from the ambient air through the aperture baffle to the 4K regime. To minimize the longitudinal temperature gradient on the optical bench or optical components, eight high purity (RRR=1,000) aluminum busbars are used to increase the longitudinal conductance of the inner shroud after thermal iterations. They are spaced 45° apart. Each busbar consists of 2.54 cm (1 inch) long and 0.16 cm (0.063 inch) thick strips, which are spaced 15.24 cm (6 inch) apart. The strips are welded to the inner shroud.

Because the intermediate shroud is also made of aluminum alloy 6061-T6, its conductance is not high at about 50K. As mentioned earlier, the warmer aperture baffle is mounted to and conductively coupled to the front end of the intermediate shroud. There is a radiative heat load from the ambient air outside the SOFIA aircraft through the aperture to the warmer baffle. To minimize the longitudinal temperature gradient on the intermediate shroud, eight high purity (RRR=1,000) aluminum busbars are used to increase the longitudinal conductance of the intermediate shroud after thermal iterations. They are spaced 45° apart. Each busbar consists of 2.54 cm (1 inch) long and 0.16 cm (0.063 inch) thick strips, which are spaced 15.24 cm (6 inch) apart. The strips are welded to the intermediate shroud.

F. Method of Minimizing Radiative Parasitic Heat Loads

Dewar multilayer insulation (MLI) blankets cover the interior of the intermediate shroud and ring and the interior of the outer shroud and ring. Lockheed Martin Space Company (LMSC) measured the effective emittance

(e*) of a sample dewar MLI with 37 layers of doubled coated aluminized Kapton and single silk netting. Figure 16 shows the results of the measurements.[7] The silk nets were home made. Because silk net is not commercially available, double dacron netting is used for the HIRMES MLI to reduce cost. The MLI conisists of 37 layers of doubled coated aluminized mylar and double dacron netting separators. With exception of the outer cover, all layers are 0.0085 mm (0.333 mil) thick. The thickness of the outer cover is 0.0508 mm (2 mil). Some areas have MLI blanket overlaps. The number of MLI layers for the overlaps is reduced to 18 or 19 each, so that the total number does not exceed 37. The separations between the inner and intermediate shrouds, and between the intermediate and outer shrouds are adequate to accommodate such a thick MLI. Figure 17 shows a sample of the HIRMES MLI blankets.

The e* versus hot side temperature curve in Figure 16 is used in the HIRMES thermal model to predict the heat loads without margin for the PTC first and second stages. It is then mutliplied by two in the analytical case to provide a 100% margin for the PTC heat load predictions.

The HIRMES cryostat, including MLI blankets, is cooled by PTC1 and PTC2 to cryogenics temperatures on the ground before the SOFIA aircraft takes off. Acrylic adhesives, such as pressure sensitive adhesive Y966, on Kapton tape have zero peel strength at the cryogenic temperatures of HIRMES. Generally, there is mechanical vibration during aircraft take off, in flight (especially during turbulence), and landing. To assure the integrity of the MLI blankets under these circumstances, selected edges of the MLI blankets are stitched. To minimize the contact area between the MLI blankets and inner shroud or intermediate shroud, MLI pads are added between them. The pads are bonded to the exterior of the inner shroud and intermediate shroud using a cryogenic epoxy. The MLI blankets sit on the top of the pads. This technique minimizes the heat conduction from the MLI blankets to the inner shroud or intermediate shroud through contacts.

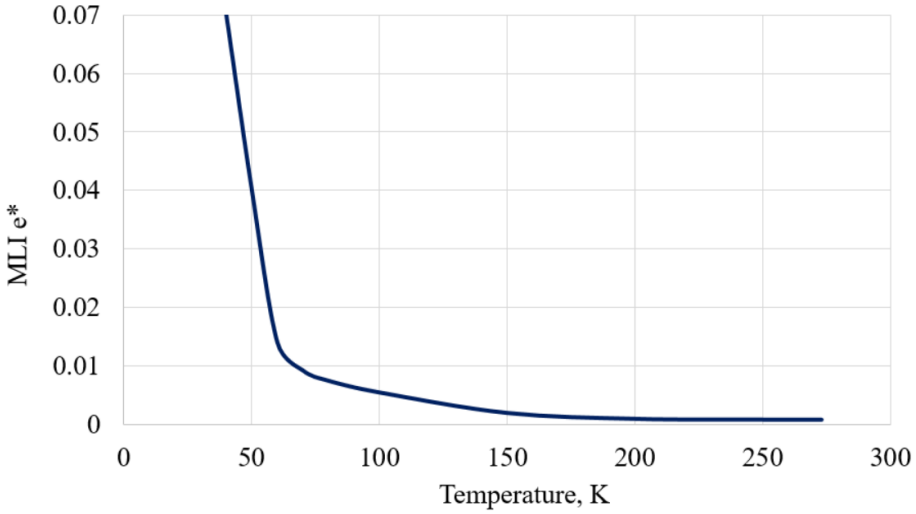

Figure 16. MLI e* versus MLI hot side temperature.[7]

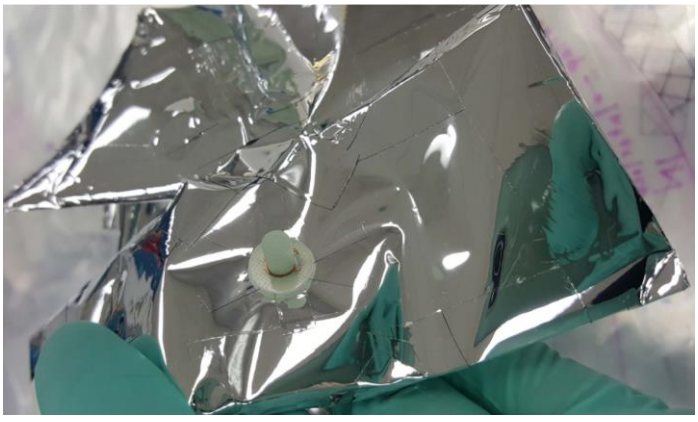

Figure 17. Sample of HIRMES MLI. (Credit: SOFIA HIRMES project)

G. Method of Minimizing Conductive Parasitic Heat Load through Harness to 4K

At steady state, the motors are powered off. There is heat conduction through the harness to the 4K regime from the avionics. In the transient mode, one of the motors is turned on. Ohmic losses in the harness conductors add heat load to the 4K regime. After thermal iterations, the harness between the outer and intermediate shrouds, and between the intermediate and inner shrouds is wrapped with high purity (RRR=1,000) annealed aluminum foils. The aluminum foils are attached to the intermediate shroud so that there is a good heat conduction path from the harness to the intermediate shroud and ring. A thermal conductance of 1 WK^{-1} is assumed. This technique assures that the harness is cooled as much as possible before it enters the 4K regime.

IV. Thermal Modeling and Analysis

Figure 18 presents the thermal block diagram for the thermal design presented in Section III. It shows the three shrouds (outer, intermediate, and inner), the hexapod structure, the MLI between the shrouds, the aperture, the optical bench, the optical components, the 3He/4He sorption cooler, the cryocoolers (PTC1 and PTC2), the harness, the thermal doublers, the thermal busbars, and the boundary temperatures inside and outside the aircraft. Both the PTC1 first stage and PTC2 first stage cool the intermediate shroud ring. The PTC1 second stage is dedicated to remove heat from the inner shroud ring. The PTC2 second stage is dedicated to remove heat from the 3He/4He sorption cooler condenser. The latter is thermally isolated from the optical bench by G10 standoffs. Based on the thermal block diagram, the MLI e* in Figure 19, the hexapod structure conductance, the copper strap conductances, the contact conductances, the conductance from the harness to the intermediate shroud, the mass in Table 1, the thermal conductivties versus temperature, the specific heats versus temperature, and the hemispherical emittance of irridited aluminum, a thermal model in Thermal Desktop format has been built (Figure 19). The solid conduction through the Ti-6Al-4V struts, CRES 416 strut ends, and CRES 303 clevises of the hexapod structure is calculated based on the dimensions and thermal conductivity. Table 3 presents the contact conductances assumed at the clevises and strut ends of the hexapod structure.

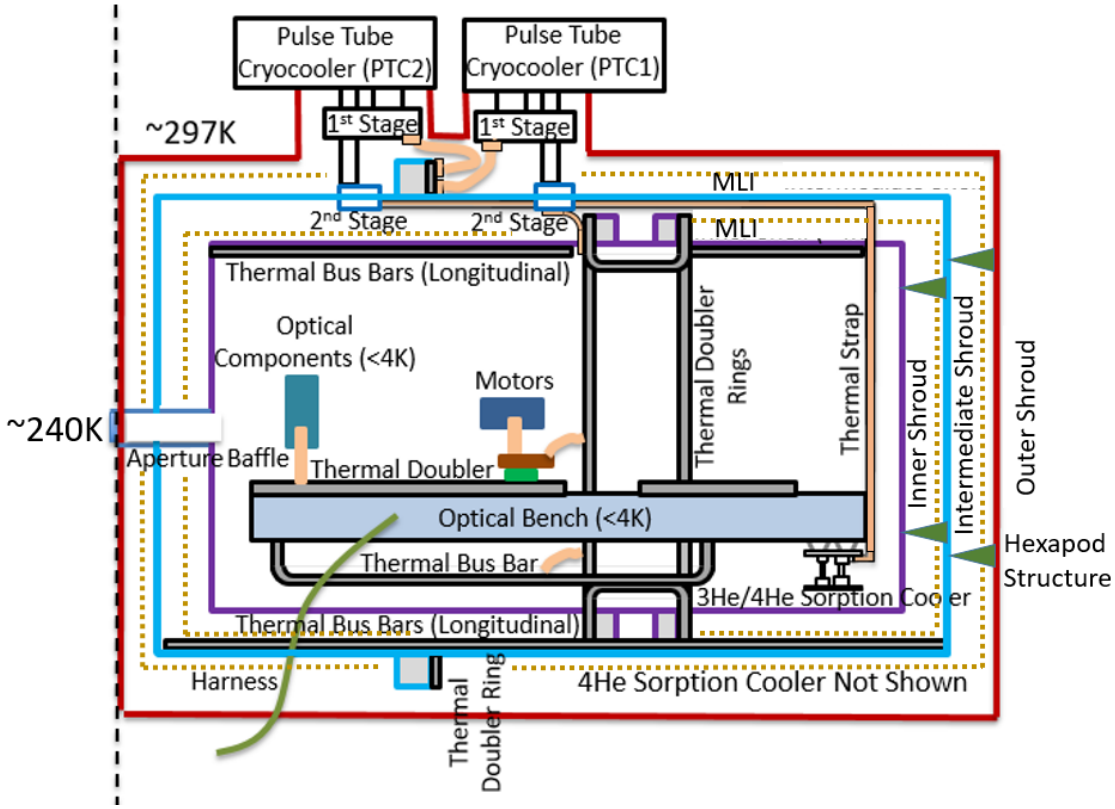

Figure 18. Thermal block diagram.

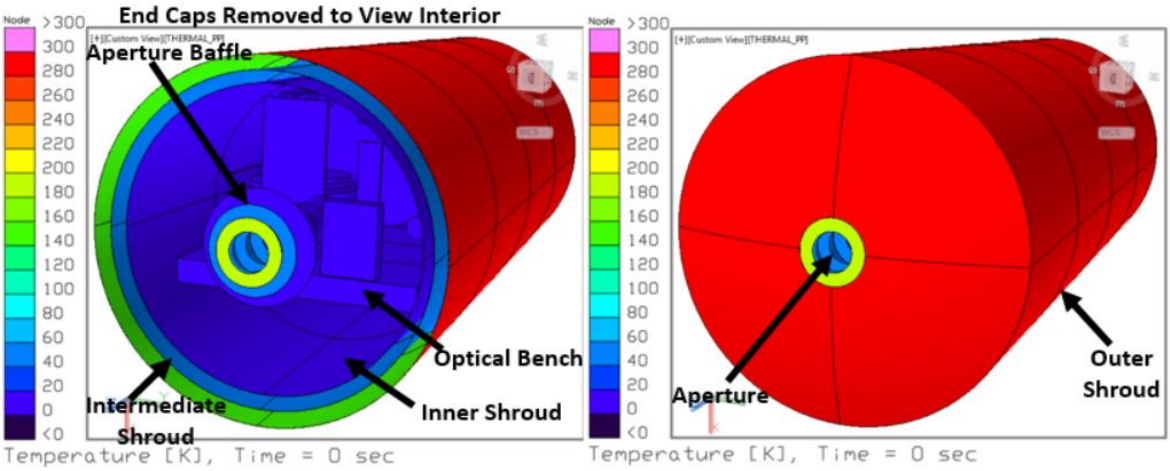

Figure 19. Thermal model.

Table 3. Contact Conductances Assumed for Each Strut of Hexapod Structure.

Component	Contact Conductance (W/K)
Clevis to Shroud Ring	0.45 each
Clevis to Strut End	0.3385 each
Strut End to Strut	0.081 each

The methodology of thermal modeling and analysis consists of two steps. In the first step, the thermal model is run to predict heat loads without margin for the PTC first and second stages at steady state. In the second step, the following parameters are iterated until the predicted heat loads at steady state are doubled. They include increasing the MLI e*, increasing the thermal conductance of the hexapod structure, increasing the thermal conductance of the harness, increasing the ambient temperature outside the aperture, and changing the optical properties of irridited aluminum and the aperture baffle interior. Table 4 shows the hemispherical emittance of irridited aluminum versus temperature assumed.[8] By comparing the thermal model predictions in the above two steps, a sensitivity of the effect of heat load on the temperatures of the optical bench and optical components is obtained. Because a 100% margin is used on the heat load to be removed by the PTC, temperature margin is not used.

Table 4. Hemispherical Emittance for Irridited Aluminum.

Temperature (K)	Emittance for No Heat Load Margin	Emittance for 100% Heat Load Margin
4	0.028	0.05
10	0.029	0.049
20	0.031	0.048
30	0.033	0.047
40	0.0352	0.046
60	0.0396	0.045
80	0.044	0.044
100	0.0484	0.0484
200	0.0792	0.0792
300	0.132	0.132

The RRR values of the copper straps were iterated before they were finalized. Table 5 lists the copper straps from the PTC cold tips to the inner shroud ring and intermediate shroud ring. Table 6 lists the copper straps from the mechanisms to the inner shroud ring. Table 7 lists the copper straps from other components to the optical bench or structure in the 4K regime. The thermal conductances in the 100-300K temperature range affect the cooldown time from 297K to 4K. Tables 8, 9, and 10 present the contact conductances for the copper straps for the PTC cold tips, the copper straps for the mechanisms, and the copper straps for other components, respectively.

Table 5. Copper Straps for PTC Cold Tips.

Component	Quantity	A/L (m)	RRR	Conductance (W/K)	
				100K-300K (Average)	4K/50K
PTC1 First Stage to Intermediate Ring	1	0.0016764	500	0.733	1.97983 (50K)
PTC2 First Stage to Intermediate Ring	1	0.0016764	500	0.733	1.97983 (50K)
PTC1 Second Stage to Inner Ring	1	0.0016764	1000	0.733	10.48085 (4K)
PTC2 Second Stage to 3He/4He Cooler	1	0.0016764	1000	0.733	10.48085 (4K)

Table 6. Copper Straps for Mechanisms.

Component	Quantity	A/L (m)	RRR	Conductance (W/K)	
				100K-300K (Average)	4K
Low-res Wheel Motor	1	2.50E-06	500	1.093E-03	7.8525E-03
Mid-res Wheel Motor	1	2.50E-06	500	1.093E-03	7.8525E-03
High-res Wheel Motor	1	2.50E-06	500	1.093E-03	7.8525E-03
Filter Wheel Motor	1	2.50E-06	500	1.093E-03	7.8525E-03
Slit Wheel Motor & Shield	1	2.50E-06	500	1.093E-03	7.8525E-03
Thermal Switch Motor	1	2.50E-06	500	1.093E-03	7.8525E-03
Grating Mechanism Motor	1	2.50E-06	500	1.093E-03	7.8525E-03
Low-res Wheel Rotating Assembly	1	2.50E-06	500	1.093E-03	7.8525E-03
Low-res Wheel Clock Spring	1	2.50E-06	500	1.093E-03	7.8525E-03

Table 7. Copper Straps for Other Components.

Component	Quantity	A/L (m)	RRR	Conductance (W/K)	
				100K-300K (Average)	4K
PAM	2	3.80E-05	100	3.230E-02	4.788E-02
Low-res Wheel Motor Shield	1	3.80E-05	100	1.615E-02	2.394E-02
Mid-res Wheel Motor Shield	1	3.80E-05	100	1.615E-02	2.394E-02
High-res Wheel Motor Shield	1	3.80E-05	100	1.615E-02	2.394E-02
Filter Wheel Motor Shield	1	3.80E-05	100	1.615E-02	2.394E-02
Thermal Switch Motor Shield	1	3.80E-05	100	1.615E-02	2.394E-02
Grating Mechanism Motor Shield	1	3.80E-05	100	1.615E-02	2.394E-02
Low-res/Filter Wheel Assembly Tie Straps	3	3.80E-05	100	4.845E-02	7.182E-02
Mid-res Wheel Rotating Assembly	1	3.80E-05	100	1.615E-02	2.394E-02
High-res Wheel Rotating Assembly	1	3.80E-05	100	1.615E-02	2.394E-02
Filter Wheel Rotating Assembly	1	3.80E-05	100	1.615E-02	2.394E-02
Slit Wheel Rotating Assembly	1	3.80E-05	100	1.615E-02	2.394E-02
Grating Mechanism Rotating Assembly	1	3.80E-05	100	1.615E-02	2.394E-02
Foreoptics Tower to OB	1	3.80E-05	100	1.615E-02	2.394E-02
Filter Wheel Tower to OB	1	3.80E-05	100	1.615E-02	2.394E-02
Mid-res Clockspring to OB	1	3.80E-05	100	1.615E-02	2.394E-02
High-res Clockspring to OB	1	3.80E-05	100	1.615E-02	2.394E-02
ADR Magnet/Structure	1	3.80E-05	100	1.615E-02	2.394E-02

Table 8. Contact Conductances for Copper Straps for PTC Cold Tips.

Component	Contact Conductance (W/K)
PTC1 First Stage to Intermediate Ring	3 at Cold Tip; 2 at Intermediate Ring
PTC2 First Stage to Intermediate Ring	3 at Cold Tip; 2 at Intermediate Ring
PTC1 Second Stage to Inner Ring	3.3 at Cold Tip; 2 at Inner Ring
PTC2 Second Stage to 3He/4He Condenser Busbar	3.3 at Cold Tip; 2 at 3He/4He Condenser Busbar

Table 9. Contact Conductances for Copper Straps for Mechanisms.

Component	Contact Conductance (W/K)
Low-res Wheel Motor	0.32 at Busbar; 0.045 at Motor
Mid-res Wheel Motor	0.32 at Busbar; 0.045 at Motor
High-res Wheel Motor	0.32 at Busbar; 0.045 at Motor
Filter Wheel Motor	0.32 at Busbar; 0.045 at Motor
Slit Wheel Motor & Shield	0.32 at Busbar; 0.045 at Motor
Thermal Switch Motor	0.32 at Busbar; 0.045 at Motor
Grating Mechanism Motor	0.32 at Busbar; 0.045 at Motor
Low-res Wheel Clock Spring	0.32 at Busbar; 0.045 at Motor

Table 10. Contact Conductances for Copper Straps for Other Components.

Component	Contact Conductance (W/K)
PAM	0.2 at Component; 0.2 at Optical Bench
Low-res Wheel Motor Shield	0.2 at Component; 0.2 at Optical Bench
Mid-res Wheel Motor Shield	0.2 at Component; 0.2 at Optical Bench
High-res Wheel Motor Shield	0.2 at Component; 0.2 at Optical Bench
Filter Wheel Motor Shield	0.2 at Component; 0.2 at Optical Bench
Thermal Switch Motor Shield	0.2 at Component; 0.2 at Optical Bench
Grating Mechanism Motor Shield	0.2 at Component; 0.2 at Optical Bench
Low-res/Filter wheel assembly tie straps	0.2 at Component; 0.2 at Optical Bench
Mid-res Wheel Rotating Assembly	0.2 at Component; 0.2 at Optical Bench
High-res Wheel Rotating Assembly	0.2 at Component; 0.2 at Optical Bench
Filter Wheel Rotating Assembly	0.2 at Component; 0.2 at Optical Bench
Slit Wheel Rotating Assembly	0.2 at Component; 0.2 at Optical Bench
Grating Mechanism Rotating Assembly	0.2 at Component; 0.2 at Optical Bench
Foreoptics Tower to Optical Bench	0.2 at Component; 0.2 at Optical Bench
Filter Wheel Tower to Optical Bench	0.2 at Component; 0.2 at Optical Bench
Mid-res Clockspring to Optical Bench	0.2 at Component; 0.2 at Optical Bench
High-res Clockspring to Optical Bench	0.2 at Component; 0.2 at Optical Bench
ADR Magnet/Structure	0.2 at ADR; 0.2 at Optical Bench

V. Thermal Predictions

From the thermal model predictions, there are four sources of heat loads. The first one is heat conduction from the warmer shroud to the colder shroud through the hexapod structure. The second one is heat radiation from the warmer shroud to the colder shroud through the MLI blankets. The third one is heat radiation from the ambient air outside the SOFIA aircraft through the aperture to the aperture baffle and 4K components. The fourth one is heat conduction from the avionics to the 4K components and intermediate shroud through the harness.

A. Steady State Case

Figure 20 presents the temperature and heat load predictions for the steady state case with a 100% heat load margin. The temperature predictions of the optical bench and optical components are 3.6K. They meet the thermal requirement. The heat load prediction for the PTC1 second stage is 0.305 W. Heat conduction from the intermediate shroud through the hexapod structure to the inner shroud contributes 57.6% of this heat load. Heat radiation from the ambient air outside the aircraft through the aperture and from the aperture baffle tube to the 4K regime contributes 29.9%. Heat radiation from the intermediate shroud to the inner shroud and ring through the MLI blankets contributes 9.6%. Heat conduction from the intermediate shroud to the 4K regime through the harness contributes 2.9%. The heat load prediction for the PTC2 second stage is only 0.009 W. The reason is that the 3He/4He sorption cooler is thermally isolated from the optical bench and it does not dissipate heat during the steady state condition. The heat load prediction for the intermediate shroud and ring is 9.334 W. Heat conduction from the outer shroud to the intermediate shroud through the hexapod structure contributes 39.9% of this heat load. Heat radiation from the outer shroud to the intermediate shroud through the MLI blankets contributes 34.9%. Heat radiation from the ambient air outside the aircraft to the aperture baffle through the aperture contributes 7.2%. Heat conduction from the avionics to the intermediate shroud through the harness contributes 18%. Because the heat leak from the intermediate shroud and ring to the optical bench, optical components, and inner shroud and ring is 0.241 W, the heat load prediction for the PTC1 first stage and PTC2 first stage is 9.093 W. PTC1 and PTC2 remove 47% and 53%, respectively, of this heat load.

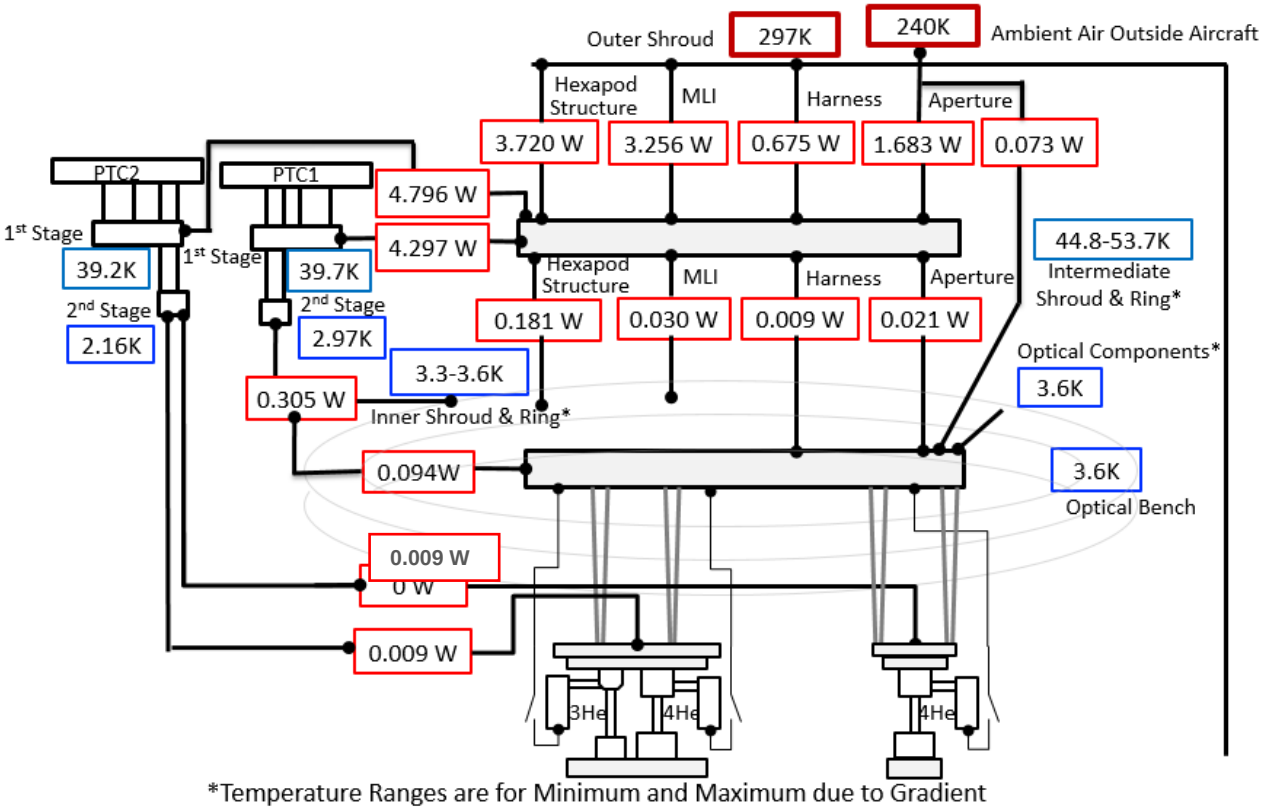

Figure 20. Thermal predictions at steady state with 100% heat load margin.

The temperature predictions for the second stage cold tips of PTC1 and PTC2 are 2.97K and 2.16K, respectively. The temperature predictions for the first stage cold tips of PTC1 and PTC2 are 39.7K and 39.2K, respectively. Figure 21 shows the location of the design points of PTC1 and PTC2 on the load map. The temperature prediction for the inner shroud and ring is 3.3K minimum and 3.6K maximum. Therefore, there is a 0.3K temperature gradient. The temperature prediction for the intermediate shroud and ring is 44.8K minimum and 53.7K maximum. Therefore, there is an 8.9K temperature gradient.

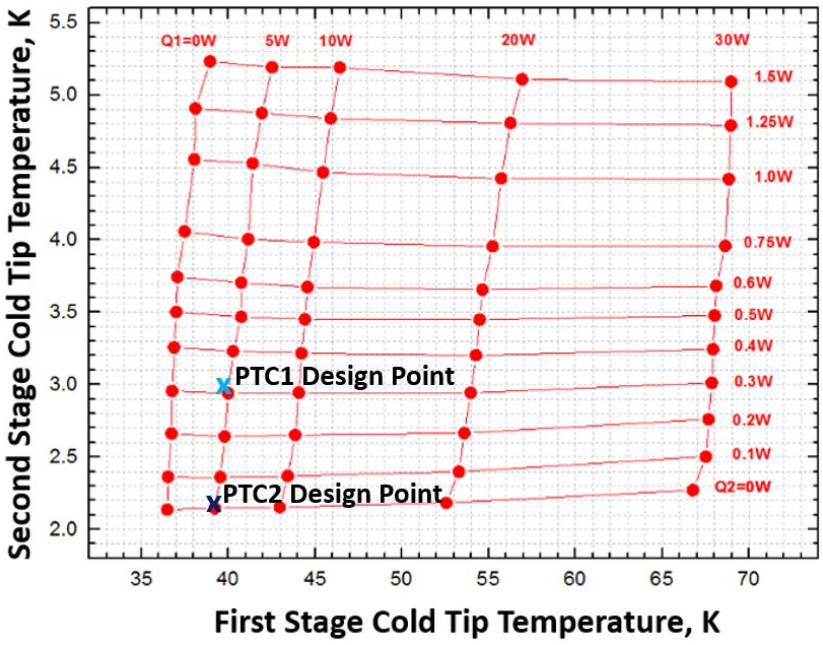

Figure 21. PTC design points at steady state with 100% heat load margin.

B. Cooldown from 297K to Steady State Temperatures

The PTCs are powered on to cool HIRMES from approximately 297K to steady state temperatures before it is translated from the hangar to the SOFIA aircraft. Figure 22 shows cooldown curves for selected optical components, mechanisms, and optical bench in the 4K regime. The predicted cooldown time is 8.7 days. The large mass of 208.9 kg in the 4K regime and large thermal resistance between the components on the optical bench and PTC second stage cold tips cause the long cooldown time. The time for cooling from 297K to 100K is the majority of the cooldown time because the specific heats begin to decrease sharply at temperatures colder than 100K (Figure 5).

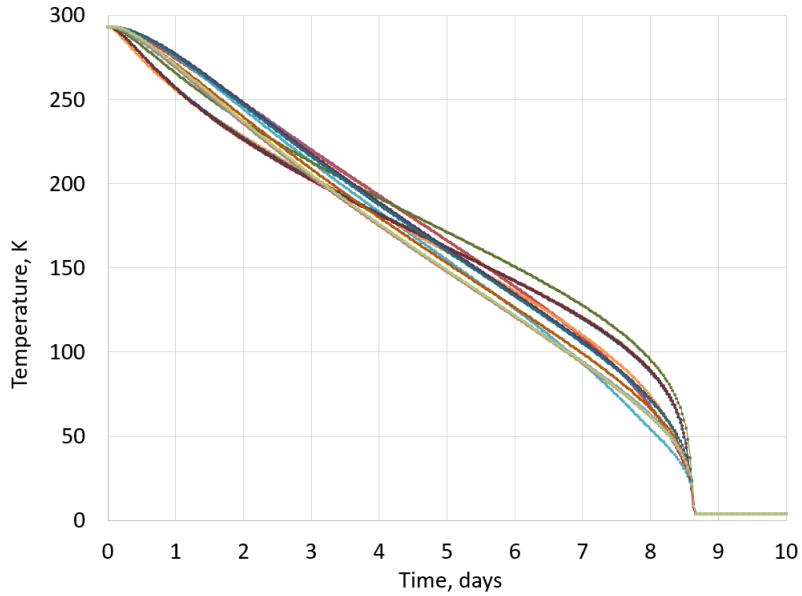

Figure 22. Cooldown from 297K to 4K.

C. Transient Case after Cooldown

There are two conditions that affect the heat loads to the PTCs transiently after the cooldown to 4K. The first condition is when a motor is turned on for up to 90 seconds during the science mode. The maximum power dissipation of the motors is 400 mW. The time interval for turning on one of the nine motors in the flight operation

plan is 30-60 minutes. Figure 23 shows the transient temperature prediction for the warmest optical component when a motor is powered on for 90 seconds. The temperature prediction for this optical component increases to a maximum of 3.8K from 3.4K. When a motor is turned on, the ohmic loss in the leads is estimated to be 40 mW. It adds 0.03K to the temperature prediction for this optical component after 90 seconds. Because the ohmic loss in the harness is an order of magnitude smaller than the motor power dissipation, its thermal effect is small. There is no need to wait for the optical components to cool down to 4K. The temperature prediction of the warmest optical component begins to stabilize at 4K after 20 minutes. At that time, another motor can be turned on. The 20 minutes waiting time is consistent with the motor actuation plan.

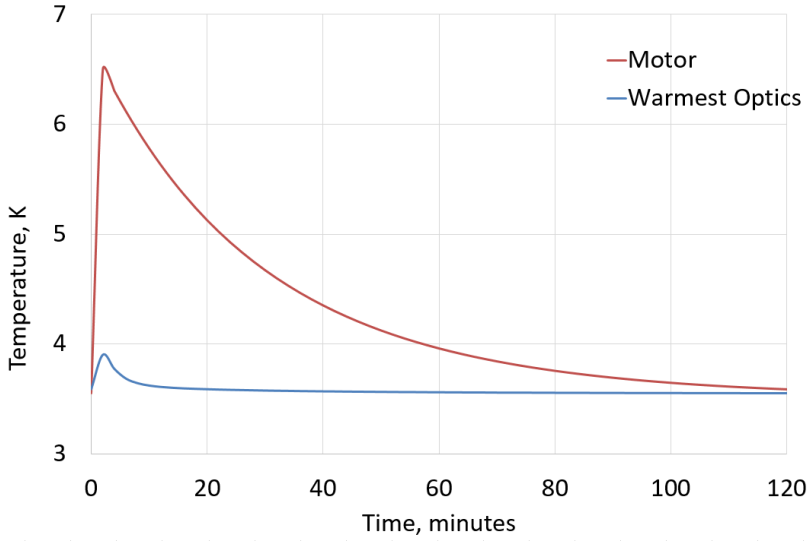

Figure 23. Transient temperature of motor and optics during motor turn on.

The second condition is when there is a power outage for up to 45 minutes during the flight day. An example of power outage is during the translation of HIRMES from the hangar to the SOFIA aircraft. According to the PTC manufacturer, when the PTC is powered off, the parasitic heat loads from its thermomechanical unit to the first stage and second stage are 5.5 W and 0.239 W, respectively. They are included in the thermal model for this transient condition. Figure 24 shows the transient temperature prediction for the warmest optical component when the PTCs are powered off for 45 minutes. The temperature prediction for this optical component increases to a maximum of 9K. At the end of the 45 minutes, the PTCs are powered on again. The temperature prediction for this optical component reaches 4K after 15 minutes.

The transient heat loads in the above two conditions have low risk to the temperatures of the optical components or optical bench.

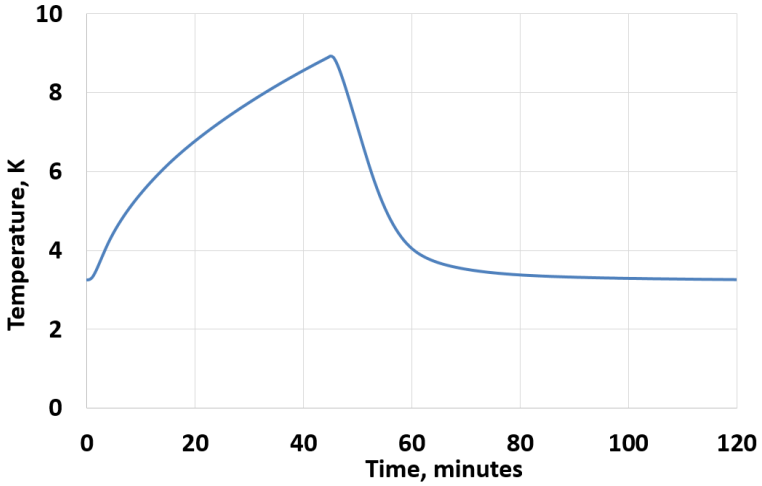

Figure 24. Transient temperature of optical components for 45 minutes power outage.

VI. Conclusion

This paper has presented the SOFIA HIRMES thermal design approach to meet the 4K maximum temperature limit requirement for the optical bench and optical components. A 100% heat load margin is used, in lieu of temperature margin. The results of thermal analysis show that the 4K stage of the thermal subsystem meets all of its requirements, using conservative modeling assumptions. The technical risk for this subsystem is low. The predicted cooldown time from 297K to 4K is 8.7 days. The time for cooling from 297K to 100K is the majority of the cooldown time. Two factors cause the long cooldown time. The first one is the large mass of 208.9 kg in the 4K regime that leads to high thermal inertia in the 100K to 297K temperature range. The second one is the large thermal resistance between the components on the optical bench and PTC second stage cold tips, especially in the 100K to 297K temperature range. An instrument level thermal balance test will be performed to verify the thermal design and to correlate the thermal model. It includes a steady state case and three transient cases. The first transient case is a cooldown from 297K to 4K steady state temperatures. The second transient case is to simulate a motor turned on for 90 seconds. The third transient case is to simulate a power outage for 45 minutes.

Acknowledgments

The author thanks the following individuals for their technical contributions: James Kellogg and LeRoy Sparr of GSFC Code 592; Amir Jahromi, Robert Boyle, and Stuart Banks of GSFC Code 552.

References

[1]Richards, S. N., et al., “SOFIA - HIRMES: Looking forward to the HIgh-Resolution Mid-infrarEd Spectrometer”, Journal of Astronomical Instrumentation, SOFIA Special Edition 2018.

[2]Ekin, J. W., Experimental Techniques for Low Temperature Measurements, Oxford University Press, Oxford, 2006.

[3]CRYOCOMP® is a database code of the state and thermal properties for technical materials.

[4]Woodcraft, A. L. "Predicting the thermal conductivity of aluminium alloys in the cryogenic to room temperature range", Cryogenics 45.6 (2005): 421-431.

[5]Powell, R. L. and Fickett, F. R., Cryogenic Properties of Copper, International Copper Research Association, Dec. 1979.

[6]Russenschuck, S., “Field Computation for Accelerator Magnets”, pp. 703-715, WILEY-VCH Verlag GmbH & Co. KGaA, Weinheim, 2010.

[7]Ross, R. G., Cryocoolers for Space Applications #2, p. 2-35, 2015 CEC Cryocooler Short Course, June 2015.

[8]Tuttle, J., et al., Thermal Properties Of Double-Aluminized Kapton At Low Temperatures, AIP Conference Proceedings 986, 34 (2008).